Multiparametric *in vivo* ultrasound shear wave viscoelastography on farm-raised fatty duck livers: human radiology imaging applied to food sciences

Manish Bhatt,[*] Ladan Yazdani,[*,†] François Destrempes,[*] Louise Allard,[*] Bich N. Nguyen,[‡] An Tang,[†,§,#] and Guy Cloutier[*,†,#,1]

[*]*Laboratory of Biorheology and Medical Ultrasonics, University of Montreal Hospital Research Center (CRCHUM), Montréal, Québec, Canada H2X 0A9;* [†]*Institute of Biomedical Engineering, University of Montreal, Montréal, Québec, Canada H3C 3J7;* [‡]*Service of Pathology, University of Montreal Hospital (CHUM), Montréal, Québec, Canada H2X 0C1;* [§]*Laboratory of Medical Image Analysis, CRCHUM, Montréal, Québec, Canada H2X 0A9; and* [#]*Department of Radiology, Radio-Oncology and Nuclear Medicine, University of Montreal, Montréal, Québec, Canada H3T 1J4*

ABSTRACT Nine mulard ducks that were being raised for foie gras (steatosis) production went through in vivo shear wave (**SW**) elastography imaging of their liver during the force-feeding period to investigate changes in liver tissue characteristics. A total of 4 imaging sessions at an interval of 3 to 4 d were conducted at the farm on each animal. Three ducks were sacrificed at the second, third, and fourth imaging sessions for histopathology analysis of all animals at these time points. Six SW elastography parameters were evaluated: SW speed, SW attenuation, SW dispersion, Young's modulus, viscosity, and shear modulus. Shear waves of different frequencies propagate with different phase velocities. Thus, SW speed and other dependent parameters such as Young's modulus, viscosity, and shear modulus were computed at 2 frequencies: 75 and 202 Hz. Each parameter depicted a statistically significant trend along the force-feeding process (P-values between 0.001 and 0.0001). The fat fraction of the liver increased over the 12-day period of feeding. All parameters increased monotonically over time at 75 Hz, whereas modal relations were seen at 202 Hz. Shear wave dispersion measured between 75 and 202 Hz depicted a plateau from day 5. Based on this validation, proposed imaging methods are aimed to be used in the future on naturally fed ducks and geese.

Key words: duck, ultrasonography, shear wave elastography, fatty liver, tissue viscoelasticity

2021 Poultry Science 100:100968
https://doi.org/10.1016/j.psj.2020.12.065

INTRODUCTION

In humans, the natural history leading from nonalcoholic fatty liver disease (**NAFLD**) to nonalcoholic steatohepatitis (**NASH**) is not completely understood; hence, there is a need to improve the noninvasive characterization of the fatty liver disease spectrum to improve diagnosis and prognosis of NAFLD. Current clinical methods for NAFLD diagnosis include liver biopsy (Sanyal et al., 2011), computed tomography (Ricci et al., 1997), and magnetic resonance-based techniques (Bonekamp et al., 2014; Gharib et al., 2017; Park et al., 2017; Qu et al., 2019). However, these methods have drawbacks such as biopsy being invasive, computed tomography being associated with ionizing radiation, and magnetic resonance imaging being expensive and not widely available. Alternatively, shear wave (**SW**) elastography is a technology based on the generation and monitoring of the SW propagation in biological tissues using an external ultrasound probe. With this technique, the targeted tissue is imaged with an ultrasound probe that first focuses an acoustic radiation force to induce tissue motion in the form of SW, and then the same probe tracks the displacement of the tissue with motion tracking algorithms. In general, the technique aims at estimating the stiffness of the tissue by monitoring the propagation speed of SW inside it. Shear waves propagate faster in stiffer media than softer materials. Ultrasound SW elastography has shown potential to emerge as a noninvasive, non-ionizing, and cheaper alternative to these techniques. Further study of in vivo animal models verified by histology could strengthen this research field and provide validated imaging alternatives for human diagnosis.

Received September 23, 2020.
Accepted December 18, 2020.

[1]Corresponding author: guy.cloutier@umontreal.ca

Ultrasound elastography has provided important datasets on human liver fibrosis and steatosis (Deffieux et al., 2015; Nightingale et al., 2015; Loomba, 2018; Parker et al., 2018). Typically, SW elastography is used to assess the shear wave speed (**SWS**) or Young's modulus as a measure of liver stiffness (Osaki et al., 2010; Ferraiolli et al., 2014; Yoon et al., 2014; Franchi-Abella et al., 2016; Song et al., 2016; Carrascal et al., 2017; Palmeri, 2019). Recent attention has also been given to SW attenuation as a measure of acoustic energy dispersion characteristics of a tissue (Bernard et al., 2016; Nenadic et al., 2017; Sharma et al., 2019). Shear wave speed dispersion, shear modulus, and viscosity are other parameters that have been explored to quantify the lossy nature of biological tissues (Barry et al., 2012; Kazemirad et al., 2016; Bhatt et al., 2019).

Another recent application of SW liver elastography is in the field of foie gras production. Fatty duck liver or foie gras is a distinctive gastronomical heritage of the French culture (Cherry, 2016). The production of foie gras involves force-feeding of ducks or geese causing the birds' liver to induce hepatic lipidosis or steatosis (Baeza et al., 2013; Bonnefont et al., 2019). Geese and wild ducks have the ability to develop foie gras naturally to store energy for migration. This process is reversible and the liver rapidly returns to a non-steatotic state during fasting. Some producers have recently developed natural feeding strategies for foie gras but commercial successes of farm-raised animals are limited due to variability in food intake and improper timing of sacrifice (Zeldovich, 2019). There is currently no in vivo method available for assessing the fatty liver state in alive birds. A noninvasive approach that would predict the fatty liver content in vivo would be beneficial to promote the transition toward foie gras production without gavage. Recently, Gesnik et al. (2020) combined shear wave elastography (**SWE**) with quantitative ultrasound (**QUS**) imaging for classification of farm-raised duck fatty liver tissues. However, their study focused only on evaluating SWS for elastic characterization of the liver tissues. Although promising, the radiation force sequence with 3 pushes did not allow assessing the SWS toward the end of the feeding process in some animals, due to poor signal-to-noise ratios (**SNR**) attributed to highly fatty tissues in that study. To improve the SNR, the number of focusing acoustic excitation pushes was increased to 5 in the current study. No additional SW elastography parameters were evaluated in the latter study. Also, in Gesnik et al. (2020), histology was available for only 1 duck sample sacrificed on day 14. Due to these data limitations, their study could not provide a broader characterization of in vivo fatty liver tissue mechanical properties that relate to tissue viscoelasticity.

Our new study proposes to estimate 6 mechanical properties of fatty duck livers in vivo that characterizes not only elastic parameters, but also the viscous characteristics of liver tissues. Ducks were raised in a farm during the fall season for commercial production of foie gras. Mechanical features assessed are SWS, SW attenuation, SWS dispersion, Young's modulus, viscosity, and shear modulus. Four of these parameters are reported for the first time in alive mulard ducks' liver. These parameters were not evaluated in the previous study by Gesnik et al. (2020). The addition of new viscoelastic parameters provides more insights for monitoring foie gras fatty liver growth. The study comprises histopathological classification of liver tissues at various time points for each duck used in this study. Ultrasound acquisitions were performed at the farm during the force-feeding process.

MATERIALS AND METHODS

Animal Procedure

This study was approved by the Institutional Animal Ethical Care Committee of the University of Montreal Hospital Research Center. Nine mulard ducks raised in a farmhouse for foie gras production were included. They were housed collectively and had free access to water. The feeding protocol is briefly discussed here. Ducks were allowed to feed themselves freely for the first 2 wk of animal preparation, called the pre-feeding period. After pre-feeding, ducks underwent 12 d of force-feeding with re-humidified corn grains (40% water and 60% dried corn grains) in increasing amounts twice a day through a mechanical pipe. Approximately 350 g of food was given at the beginning of the force-feeding period and it reached 650 g per session toward the end.

Ultrasound measurements were performed at the farm on 4 d during force-feeding (day 1, 5, 9, and 12). Animals were awake (no anesthesia) and manually held on their back during imaging sessions that were conducted by a veterinarian. A small patch of feathers close to the liver was plucked and cleaned up with water and alcohol before applying an acoustic coupling gel for ultrasound acquisitions. This step was necessary to avoid ultrasound shadows by air trapped in feathers. The imaging session lasted about 10 min for each duck. All 9 ducks were imaged on day 1 and 5. Three ducks were sacrificed after imaging on day 5 and their liver tissue was sent for histopathology analysis. The remaining 6 ducks were imaged on day 9, and after the imaging session 3 other ducks were sacrificed for histopathology analysis. Finally on day 12, the last 3 ducks were imaged, and then sacrificed for histology.

This animal batch was a new cohort at the new season and was different from the one detailed in Gesnik et al. (2020). Experiments were carried out at a closer interval of 3 to 4 d to better monitor fat growth in livers while Gesnik et al. (2020) had conducted experiments at 1 wk interval. The new study could accommodate 4 experimental days during the force-feeding period of 2 wk. We also performed experiments with an updated scanner that allowed to acquire 4 times more data in the same acquisition time for each measurement. Thus, we could obtain a larger dataset for each duck to improve robustness, and due to this advantage we were able to evaluate additional elastography parameters.

Histology of Tissue Samples

Liver samples were placed in a 10% formalin solution within 4 min of animal euthanasia, and subsequently stained with hematoxylin and eosin, Masson's trichrome, and Sirius red. A liver pathologist assessed the histology slides according to the NASH Clinical Research Network scoring system (Kleiner et al., 2005). The pathologist's assessment included the steatosis grade (0–3), lobular inflammation (0–3), hepatocellular ballooning (0–2), and fibrosis stage (0–4). Fibrosis stage 1a was used to describe minor observation.

Ultrasound Data Acquisition

A Verasonics Vantage programmable system (Verasonics Inc., Kirkland, WA) was used to perform ultrasound measurements using an ATL L7-4 linear probe (Philips, Bothell, WA) driven at 5 MHz. The probe had 128 transducer elements in a linear array. The veterinarian positioned the probe on top of the duck liver for real-time B-mode imaging. The focus for acoustic radiation pressure pushes was selected manually at 1 cm depth within the liver. The acquisition mode was switched to SW elastography to transmit 5 pushes in the middle of the image. The focused acoustic pushes were made with 64 elements of the transducer. The ultrasound excitation voltage was fixed at 42 V. Five pushes were made altogether, that is one immediately after the other for each acquisition. Each push lasted 198.4 μs and they were positioned from −5 to 5 mm of the focal zone with steps of 2.5 mm in depth. There was a delay of 125 μs between 2 consecutive pushes. The same transducer was used to track SW immediately after their generation. One acquisition consisted of 100 radio frequency frames that were acquired for SW tracking. A total of 4 acquisitions, one immediately after the other, were recorded for each measurement on a given duck. This exercise was repeated 2 to 3 times for each duck on a given day. This was done to minimize movement artifacts by averaging mechanical parameters over all datasets of a given duck at a given time point.

A cine-loop reconstruction was performed immediately after data acquisition for visual display of B-mode images as well as SW propagation, and for assessment of image quality. Beamforming was performed using the f-k migration method (Garcia et al., 2013). For this purpose, each reconstructed frame at a pulse repetition frequency of 10,870 Hz was the compounded coherent sum of 3 angulated planes between −1° to 1°, resulting in a frame rate of 3,623 Hz for SW displacement tracking. The contour of the liver was manually outlined with inputs from the veterinarian. Radio frequency data were saved for SW elastography data post-processing.

SW Elastography

The SW velocity field inside the liver was computed using a 2-dimensional auto-correlation algorithm (Loupas et al., 1995). The liver was assumed to be locally homogeneous and computations were performed over a region-of-interest (**ROI**) of size 1 cm × 1 cm or smaller in cases the segmented contour had a smaller size because of noise. This ROI was selected in the part of the liver where lesser noisy fields were observed, usually at depths corresponding to acoustic pushes. Extracted SW mechanical parameters are described below. All post-processing steps were implemented in MATLAB (Version 2018a, MathWorks, Natick, MA).

SWS: The SW phase velocity c (also referred to as the SWS) was estimated from the velocity field that was averaged over depth z within the selected ROI. The method is similar to the one described in Deffieux et al. (2009). The phase velocity was estimated at 2 frequencies of 75 and 202 Hz. The selection was done so that one of the frequencies (75 Hz) is near the lower full-width half-maximum frequency, and the other (202 Hz) remains near the peak frequency of the SW amplitude spectrum, respectively (Figure 1). These frequencies were selected for SWS computation as they offered better SNR, and in fact, higher frequencies would have attenuated rapidly in fatty livers. Consequently, computations could not be performed at higher frequencies due to frequency-dependent attenuation giving a poor SNR. The estimation was performed by computing the slope of the linear fit of the phase vs. lateral position x, that is

$$c = \omega \Delta x / \Delta \varphi \ , \tag{1}$$

where ω is the SW angular frequency, and $\Delta\varphi$ is the phase difference occurring after the wave has traveled a distance Δx (Deffieux et al., 2009). For each SW acquisition, the goodness-of-fit of the phase velocity linear function was assessed with the coefficient of determination (R^2) (Bouchard et al., 2009; Gesnik et al., 2020). Coefficient of determination values corresponding to $R^2 < 0.95$ were not considered. The computation was performed for each acquisition and estimated SWS values were averaged to a single value for each duck.

Young's Modulus: As a measure of stiffness or elasticity, the Young's modulus E was computed using the relation

$$E = 3\rho c^2, \tag{2}$$

where ρ is the tissue mass density assumed to be 1,050 kg/m^3, and c is the SWS. Even though biological tissues are known to be viscous, the Young's modulus values were reported with the assumption of elastic and incompressible media, as has been the standard practice in liver imaging (Barry et al., 2012).

SWS Dispersion: Barry et al. (2012, 2014, 2015) studied the dispersion of the SWS and reported that it may have a correlation with the degree of liver steatosis. As the SWS (phase velocity) is a frequency-dependent measure, the dispersion was assessed as its slope vs. frequency (Barry et al., 2012; Parker et al., 2015). In this study, the SWS slope was computed between 75 and 202 Hz.

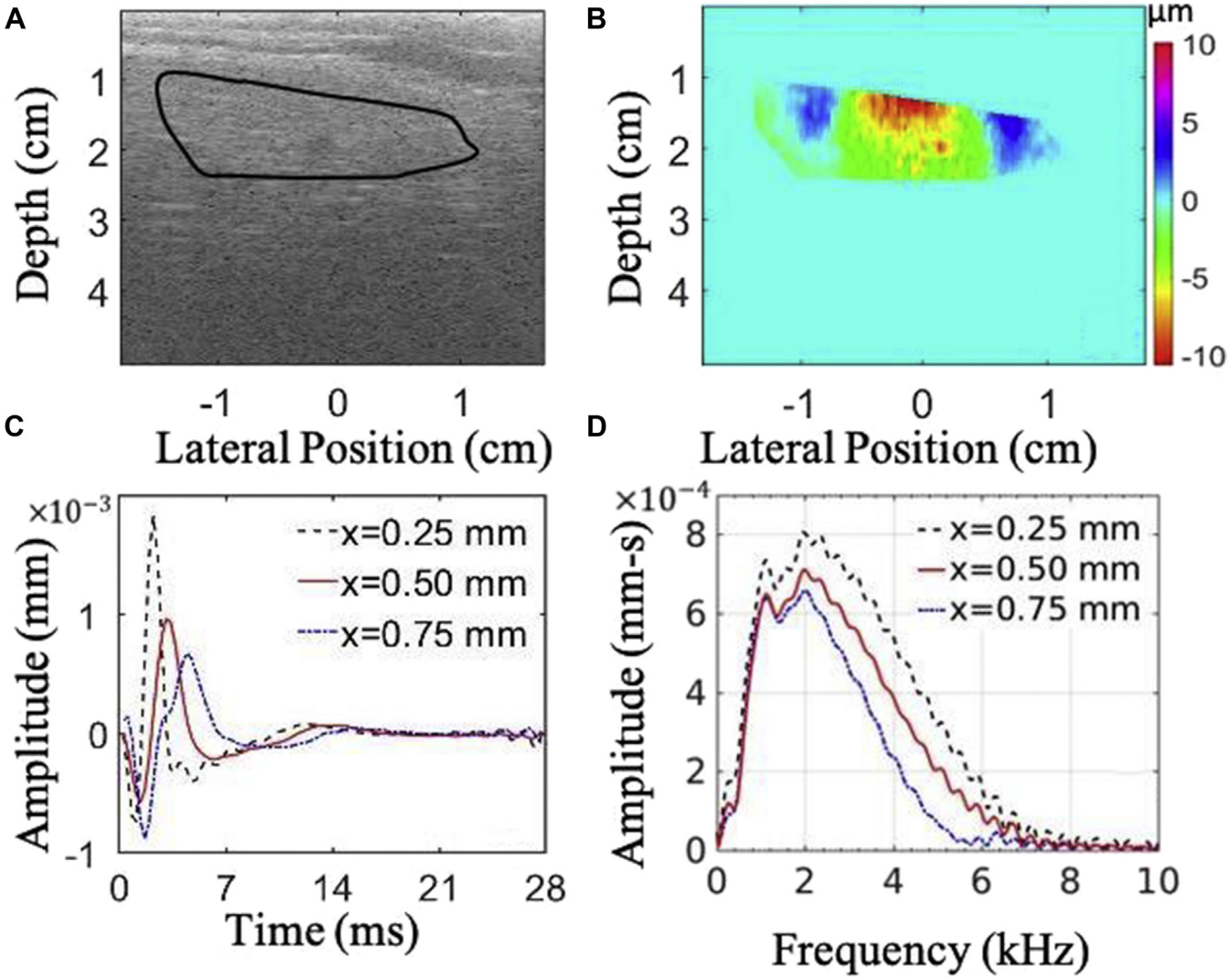

Figure 1. Illustration of acquired data at day 1. (A) In vivo B-mode image of a duck liver and segmented region of interest. (B) The segmented liver within which shear wave propagation can be seen. (C) Averaged velocity field signals in the time domain at 3 lateral positions; the attenuation in amplitude over distance can be seen. (D) Corresponding frequency domain signals at the 3 lateral positions.

SW Attenuation: The SW attenuation (α) in lossy media has been a subject of interest for assessing tissue viscoelasticity (Bernard et al., 2016; Nenadic et al., 2017; Sharma et al., 2019) because biological tissues are not purely elastic and homogeneous. In this study, we utilized the frequency-shift method for SW attenuation computation (Bernard et al., 2016). The frequency-shift model assumes the amplitude spectrum of SW to be proportional to a gamma density distribution. If a SW has a frequency spectrum $S(f)$ at a point x_0, then

$$|S(f)| \propto f^{k_0-1} e^{-f\beta_o}, \tag{3}$$

where f is the frequency, and k_0 and β_0 are the shape and rate parameters of the gamma function, respectively. The frequency spectrum at a location $x=x_0+\Delta x$ can then be written as

$$|R(f)| \propto f^{k_0-1} e^{-f(\beta_o+\alpha_0\Delta x)}. \tag{4}$$

The rate parameter in the above equation becomes $\beta(\Delta x) = \beta_o + \alpha_0\Delta x$. The SW linear attenuation coefficient (α_0) is the slope of the varying rate parameter $\beta(\Delta x)$ with respect to Δx.

A low pass filter (cutoff = 650 Hz) was applied to velocity field data to remove fluctuations due to high frequency noise. This cutoff was high enough to make sure that the gamma distribution along the frequency axis was maintained. A nonlinear least-squares algorithm (Levenberg-Marquardt) was used to estimate the shape and rate parameters (k_0 and β_0) (Bernard et al., 2016). The procedure to input initial values for the gamma distribution fit followed the log-moment estimation approach described in Destrempes and Cloutier (2013), after a change of variables resulting in a gamma distribution instead of a Nakagami distribution. Estimations were performed within the selected ROI and the mean value was reported.

Shear Modulus: The shear modulus of the imaged liver, assuming a linear and isotropic viscoelastic medium, was estimated as (Kazemirad et al., 2016)

$$|G(\omega)| = |G'(\omega) + iG''(\omega)| = \left|\rho\omega^2/k^2\right| \quad (5)$$

where G is the complex shear modulus, ω is the angular SW frequency, G' is the storage modulus, G'' is the loss modulus, ρ is the medium mass density assumed at 1,050 kg/m^3, and k is the complex wavenumber. The computation of storage and loss moduli requires local estimation of the SW attenuation coefficient (α) and SWS (c) (Amador et al., 2012; Rouze et al., 2015; Kazemirad et al., 2016)

$$G' = \rho\omega^2 c^2 \frac{\omega^2 - c^2\alpha^2}{\left(c^2\alpha^2 + \omega^2\right)^2} \quad (6)$$

$$G'' = \rho\omega^2 c^2 \frac{2\omega c\alpha}{\left(c^2\alpha^2 + \omega^2\right)^2} \quad (7)$$

Viscosity: The dynamic viscosity was estimated as $\eta = \frac{G''}{\omega}$ (Kazemirad et al., 2016; Bhatt et al., 2019). This definition assumes a linear hypothesis of viscoelasticity (or Voigt model).

Statistical Analyses

Means, SD, and coefficients of variation of SWE parameters are reported for each imaging session. Since the Shapiro-Wilk normality test failed for some of the variables, a nonparametric Kruskal-Wallis test was used to confirm statistical differences between time points (imaging sessions); corresponding P-values were reported. For Kruskal-Wallis tests that were significant, the Wilcoxon rank sum test was used for post-hoc multiple pairwise comparisons to assess statistical significance between 2 different imaging sessions. For this purpose, the Holm-Bonferroni procedure was adopted for P-value adjustment. Statistical tests were performed with software R (version x64 3.2.5, R Foundation, Vienna, Austria).

RESULTS

An in vivo B-mode image of a duck liver along with the outline of the segmented region is shown in Figure 1A. A still frame of the propagating SW inside this region is displayed in Figure 1B. Such SW could travel a few centimeters (~1–4 cm) farther from the excitation point in healthy tissues, and a few millimeters (~10 mm) farther in highly fatty tissues. Averaged velocity field signals are shown in the time domain in Figure 1C, and their amplitude spectra in the frequency domain are depicted in Figure 1D. Signals are plotted for 3 lateral positions x of 0.25, 0.50, and 0.75 mm.

Figure 2 represents the mechanical indices derived from experimental measurements, namely the SWS at 75 and 202 Hz (panels A and B), SW attenuation (panel C), and SWS dispersion (panel D), respectively. Shear wave speed progressively increased over the feeding process at 75 Hz, whereas a plateau was noticed at 202 Hz. Similarly, although not significant, the mean SW attenuation was enhanced from day 1 to 12, whereas a plateau was found for SW dispersion. Means, SD, and coefficients of variation of these parameters at each imaging session are listed in Table 1.

Figure 3 shows the trends in tissue properties derived from models considering SWS and SW attenuation measurements. This figure describes observations at 75 and 202 Hz for the Young's modulus, which represents the elasticity or stiffness of the liver, the viscosity measuring the attenuating nature of the liver, and the shear modulus providing a combined viscoelasticity score at a particular frequency. These tissue properties progressively increased over time at 75 Hz, whereas plateaus were observed at 202 Hz. Table 2 lists mean values, SD, and coefficients of variation of these parameters at each imaging session.

The pathology diagnosis of liver tissue samples acquired on day 5, 9, and 12 are listed in Table 3 along with the weights of the whole livers at the time of sacrifice. All cases showed severe diffuse steatosis (100% of the hepatocytes filled with fat) and steatohepatitis. By the end of the force-feeding process (day 12), the last 3 ducks showed inflammation grade 2 and fibrosis stage F1a. Representative digitized histopathology slides are shown in Figure 4. SWE features for the 9 tissue samples, sorted according to their inflammation and fibrosis grades, are shown in Figure 5.

DISCUSSION

A multiparametric SW elastography study was carried out in 9 mulard ducks in vivo. The objective was to monitor changes in the liver tissue behavior as ducks underwent a force-feeding process of 12 d for foie gras production. Ultrasound acquisitions were performed at the farmhouse. Six viscoelastic features at 2 SW frequencies were presented to report changes in liver tissue biomechanics over time during force-feeding, along with histopathology analyses. The study had 2 motivations: 1) to develop viscoelastic biomarkers for fatty liver grading in an animal model, and 2) to provide histology-supported information to guide interpreting ultrasound viscoelasticity measures in humans. Our group's previous study by Gesnik et al. (2020) focused mainly on QUS parameters (compression wave attenuation and homodyned-K imaging) and reported only 2 SW elastography parameters, namely the SWS and dispersion. Also, their study performed histology on only 1 duck tissue sample and thus the pathological state of the tissues along the force-feeding duration could not be reported. In comparison, this study provides a wider interpretation with 6 SW elastography parameters. In addition, histology was conducted for each duck liver

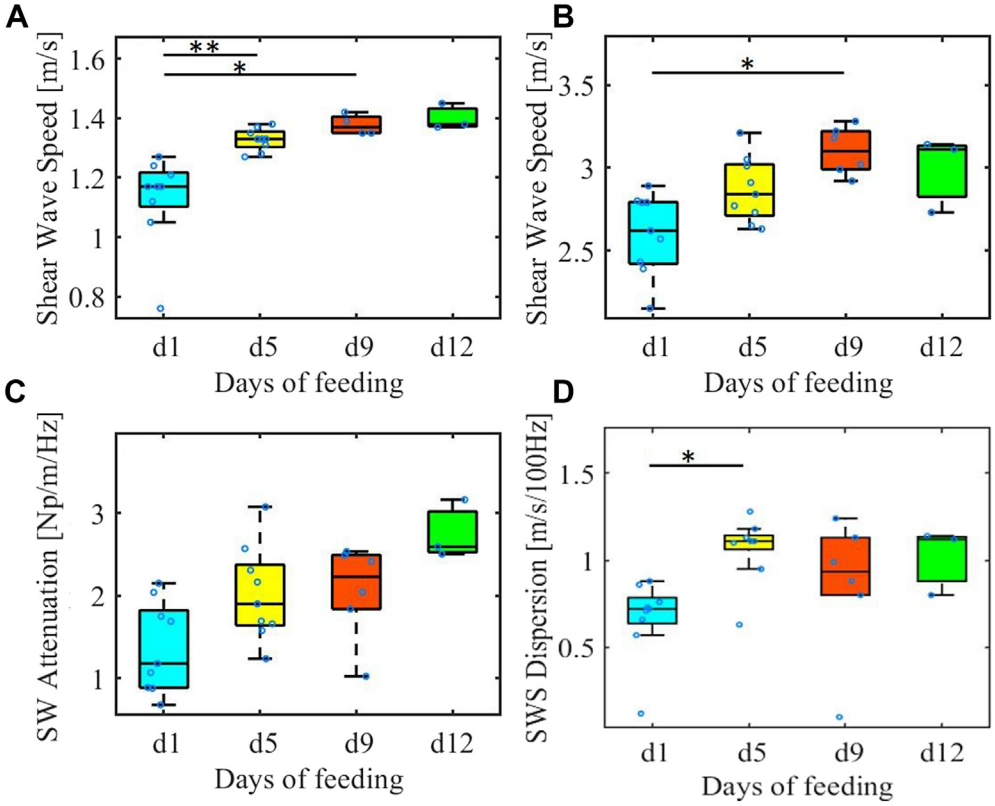

Figure 2. (A) Boxplots of the SWS observed in duck livers at the 4 time points computed at a SW frequency of 75 Hz. (B) SWS at 202 Hz. (C) SW attenuation. (D) Dispersion of the SWS. (*$P < 0.05$; **$P < 0.01$; Wilcoxon rank sum test). Abbreviations: SW, shear wave; SWS, shear wave speed.

tissue sample included in this study. The observations from these results are discussed in the following subsections.

Observations From SW Elastography Results

Shear wave propagation in tissues is dispersive due to tissue viscosity. It means that SWS in tissues is frequency dependent. Acoustic radiation force-based methods generate multifrequency SW and often dispersion is neglected in speed computation. Such systems calculate a mean SWS averaged over the frequency bandwidth of the SW, and provide an effective elasticity value assuming a purely elastic medium (Chen et al., 2013). As a result, information on tissue viscosity is lost and the effective elasticity value could be biased. On the other hand, transient ultrasound elastography utilizes a low excitation frequency of typically 50 Hz generated using an external mechanical excitation device (Sandrin et al., 2003). There is no clear agreement on which SW frequency range would provide a better distinction among different fatty liver stages. Thus, in our study, we reported viscoelasticity values at 2 different frequencies instead of a mean value.

The estimation of liver stiffness is conventionally performed with the SWS or Young's modulus. The fat percentage in the liver was assumed to increase along the force-feeding period, that is, from day 1 to 12 (Bonnefont et al., 2019; Litt et al., 2020). It should also be noted that there was a rapid increase in liver weight along this duration, as listed in Table 3. Shear wave speed estimations at 75 Hz reflected this postulate and displayed an increasing trend along the force-feeding process, suggesting that liver stiffness increased as the fat fraction increased. On the other hand, speed estimations at 202 Hz depicted a nonlinear behavior as the SWS increased up to day 9 and then plateaued at day

Table 1. Summary of the data presented in Figure 2; values from day 1 to 12 represent means over ducks per session ± 1 SD, and the coefficients of variation are given within parentheses.

Day	Day 1	Day 5	Day 9	Day 12	
Number of ducks imaged	9	9	6	3	*P*-value (Kruskal-Wallis test)
SWS (m/s; @ 75 Hz)	1.12 ± 0.15 (13.5%)	1.33 ± 0.30 (2.7%)	1.38 ± 0.03 (2.4%)	1.40 ± 0.04 (3.1%)	0.0002
SWS (m/s; @ 202 Hz)	2.60 ± 0.24 (9.3%)	2.86 ± 0.19 (6.8%)	3.10 ± 0.14 (4.6%)	2.99 ± 0.22 (7.6%)	0.0043
SW attenuation (Np/m/Hz)	1.37 ± 0.55 (39.7%)	2.02 ± 0.56 (28.0%)	2.05 ± 0.57 (27.9%)	2.75 ± 0.35 (12.9%)	0.0098
SW dispersion (m/s/100 Hz)	0.66 ± 0.22 (33.8%)	1.07 ± 0.18 (17.3%)	1.01 ± 0.16 (47.1%)	1.02 ± 0.19 (18.7%)	0.0138

Abbreviations: SW, shear wave; SWS, shear wave speed.

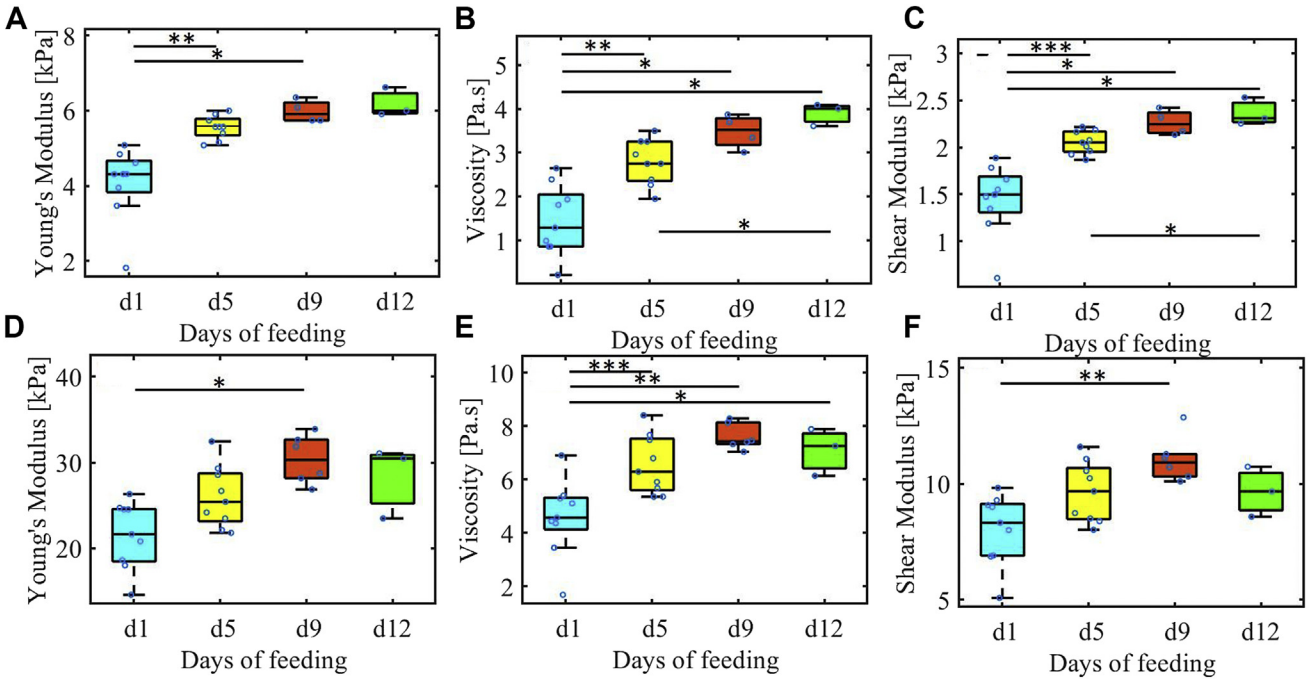

Figure 3. Boxplots for (A) Young's modulus, (B) viscosity, and (C) shear modulus observed in duck livers at 4 time points during the force-feeding process at 75 Hz. (D–F) Same boxplots estimated at 202 Hz. (*$P < 0.05$; **$P < 0.01$; ***$P < 0.001$; Wilcoxon rank sum test).

12. Although nonsignificant due to the limited sample size and high variance, SW attenuation continued to increase during this period, as shown in Figure 2C, indicating that tissues became more attenuating (and viscous) as the fat fraction increased. Parker et al. (2015) observed that steatosed livers have higher SWS dispersion than normal livers. Our results indicate the same observation that dispersion was significantly lower at day 1 compared to day 5. However, in our study, SWS dispersion could not differentiate groups of animals stratified by days of feeding, possibly because similar advanced steatosis grades occurred early in the feeding process.

Tissue mechanical properties assessed with the Young's modulus, viscosity, and shear modulus followed a similar trend as observed with the SWS. This trend also reflects a dominating dependency on phase velocity in the analytical computation of these parameters (Eqs. 6 and 7). Results were overall statistically more distinguishable at 75 Hz than at 202 Hz. Although measurements were performed at 3 to 4 d intervals, statistical significance was observed more often when there was at least a 7-day difference between 2 measurements, except for some parameters between day 1 and 5. Higher coefficients of variation were observed for SW attenuation and dispersion (Table 1), suggesting that the estimation of these 2 parameters in biological tissues has computational challenges associated with it. On the other hand, SWE parameters listed in Table 2 showed overall more variability at 202 Hz than at 75 Hz, except at day 1. This suggests that tissue lossy properties dominated with the increase in fat fraction due to force-feeding (day 5–12), and thus, computations at higher frequencies suffered. This is likely due to the fact that higher frequency SW are more prone to noise and their wave field tends to attenuate strongly or completely within a few millimeters of travel distance in the liver.

The nonlinear behavior as a function of feeding time at 202 Hz can be attributed to the frequency-dependent rheological property of fatty livers. Mean storage and loss moduli for all datasets at the 4 measurement time points are shown in Figure 6 (ANOVA on slope values vs. feeding time resulted in a P-value [Kruskal-Wallis test] of 0.011 for storage moduli and 0.001 for loss moduli,

Table 2. Summary of data presented in Figure 3; values from day 1 to 12 represent means over ducks per session ± 1 SD, and coefficients of variation are given in parentheses.

Day		Day 1	Day 5	Day 9	Day 12	
n (number of imaged ducks)		9	9	6	3	P-value (Kruskal-Wallis test)
Young's modulus (kPa)		4.07 ± 0.96 (23.8%)	5.55 ± 0.30 (5.6%)	5.97 ± 0.29 (5.0%)	6.17 ± 0.38 (6.3%)	0.0002
Viscosity (Pa•s)	75 Hz	1.44 ± 0.80 (55.6%)	2.78 ± 0.51 (18.4%)	3.48 ± 0.38 (5.9%)	3.90 ± 0.25 (6.6%)	0.0003
Shear modulus (kPa)	75 Hz	1.44 ± 0.37 (26.1%)	2.05 ± 0.12 (5.9%)	2.26 ± 0.13 (11.0%)	2.36 ± 0.14 (6.2%)	0.0001
Young's modulus (kPa)	75 Hz	21.51 ± 3.88 (18.1%)	25.99 ± 3.57 (13.8%)	30.35 ± 2.81 (9.3%)	28.33 ± 4.21 (14.9%)	0.0043
Viscosity (Pa•s)	202 Hz	4.58 ± 1.44 (31.4%)	6.55 ± 1.10 (16.8%)	7.61 ± 0.49 (6.5%)	7.09 ± 0.88 (12.5%)	0.0002
Shear modulus (kPa)	202 Hz	8.04 ± 1.51 (18.8%)	9.64 ± 1.29 (13.4%)	11.10 ± 0.98 (8.9%)	9.66 ± 1.07 (11.2%)	0.0084

Table 3. Histology characterization of liver tissue samples.

Sacrificed on day	Liver weight (g)	Steatosis	Ballooning	Inflammation	Fibrosis	Steatosis type
5	168	3	0	1	F0	Micro-steatosis
5	247	3	0	2	F0	Mixed steatosis
5	267	3	0	1	F1a	Micro-steatosis
9	327	3	0	1	F1a	Micro-steatosis
9	322	3	0	1	F0	Mixed steatosis
9	384	3	0	2	F1a	Mixed steatosis
12	654	3	0	2	F1a	Macro-steatosis
12	651	3	0	2	F1a	Macro-steatosis
12	569	3	0	2	F1a	Macro-steatosis

indicating their statistical significance). Multiple comparisons test was also performed to determine if each group (time points) mean was different from the others and *P*-values were always less than 0.001, indicating that slopes at each time point are statistically different from the others. On the first day of force-feeding (day 1), the storage modulus at 202 Hz was higher compared to 75 Hz. However, as force-feeding continued and fat accumulated in the liver tissue, the frequency dependence of the storage modulus was reduced. This means that the storage modulus varied less with frequency in highly fatty tissues. On the other hand, the loss modulus at 202 Hz was observed to be quite high compared to 75 Hz at all time points, meaning that tissue attenuating properties

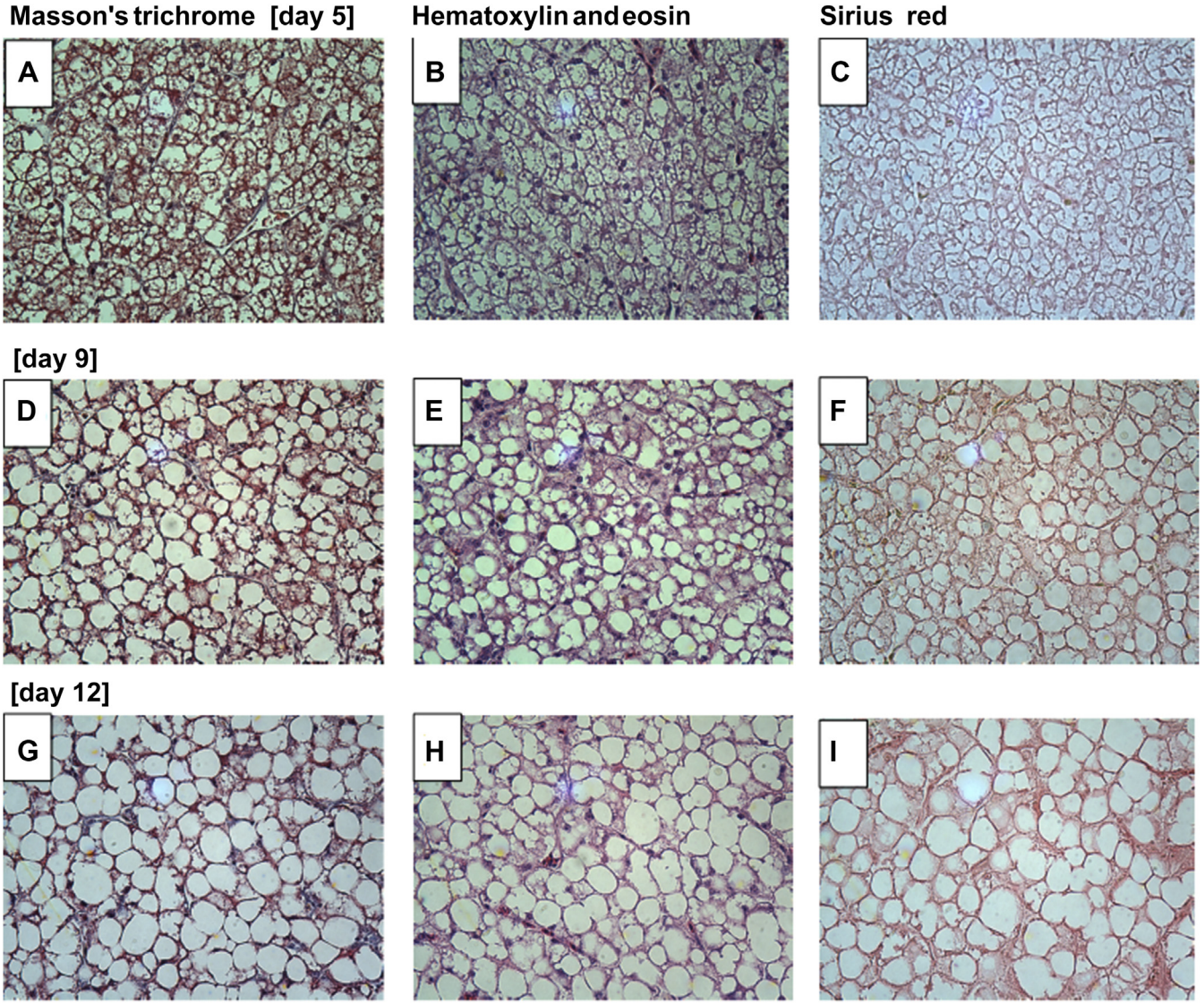

Figure 4. Histopathology slides (magnification ×40) of 3 duck liver tissue samples with Masson's trichrome stain (A, D, G), hematoxylin and eosin stain (B, E, H), and Sirius red stain (C, F, I). (A-C) The 3 stained slides for the duck sacrificed on day 5 that had micro-steatosis, inflammation grade 1, and fibrosis stage F0. (D-F) Duck sacrificed on day 9 that had mixed steatosis, inflammation grade 2, and fibrosis stage F1a. (G-I) Duck sacrificed on day 12 that had macro-steatosis, inflammation grade 2, and fibrosis stage F1a.

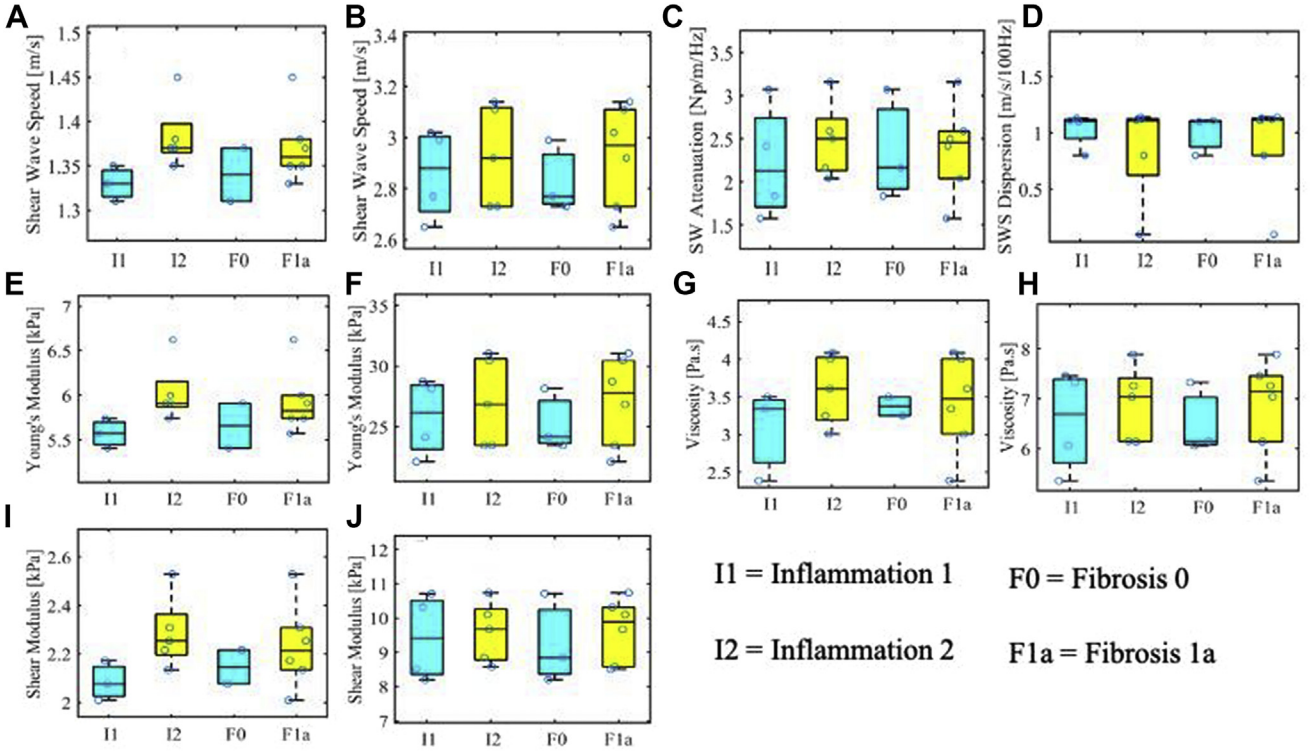

Figure 5. Comparison of shear wave elastography parameters between samples with inflammation grades 1 and 2, and between fibrosis stages F0 and F1a. (A, B) SW speed at 75 and 202 Hz, respectively, (C) SW attenuation, (D) SWS dispersion, (E, F) Young's modulus at 75 and 202 Hz, respectively, (G, H) viscosity at 75 and 202 Hz, respectively, and (I, J) shear modulus at 75 and 202 Hz, respectively. No statistically significant results were found. Green and yellow colors are used for visual purpose to depict different grades of inflammation or fibrosis. Abbreviations: SW, shear wave; SWS, shear wave speed.

got dominated by fat accumulation. This suggests that the increase in fat percentage is attributed to high losses at higher frequencies. The loss modulus slope increased from day 1 to 5 to 9 but then decreased from day 9 to 12, as seen in Figure 6B, which explains the observed plateaus in tissue properties at 202 Hz. Interestingly, similar nonlinear observations in compression wave analysis were also reported in a clinical study on human livers where tissues exhibited nonlinear variations at higher fat fractions (Han et al., 2019).

In our previous study by Gesnik et al. (2020), elastography parameters could not be computed toward the end

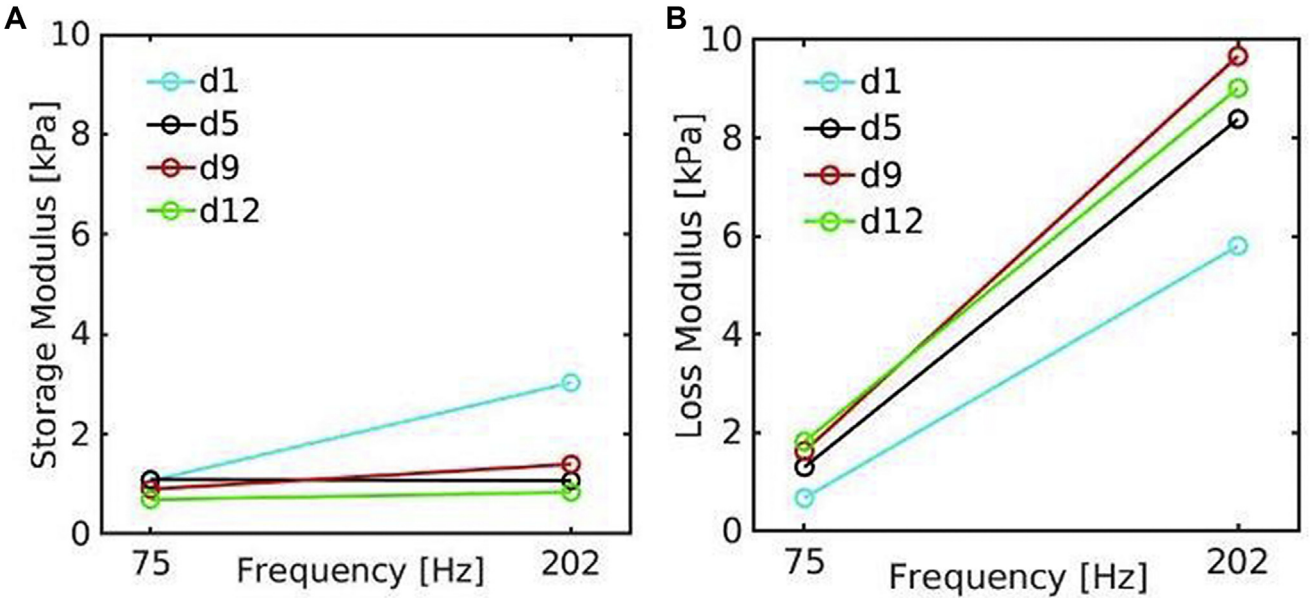

Figure 6. Mean (A) storage modulus and (B) loss modulus values for all ducks' data at 75 and 202 Hz at the 4 measurement time points. Abbreviations: d1, day 1; d5, day 5; d9, day 9; d12, day 12.

of the feeding process for ∼ 50% of the animals due to poor SNR at the selected higher SW frequency of 400 Hz. However, in the current study, we chose to perform computations at lower SW frequencies to overcome the SNR challenges. Computations at lower frequencies allowed measurements to be performed for all animals and could provide wider characterization of liver tissues with 6 elastography parameters. It should also be noted that our study also faced the low SNR challenge at higher frequencies and did not provide meaningful interpretations at 400 Hz. Thus, a significant observation from this study is that in vivo computations in duck fatty liver models should be performed at lower frequencies to overcome background noise challenges.

Observations From Histopathology Analysis

Three samples were collected on day 5, 9, and 12. The mean weights of the livers at the time of sacrifice on day 5, 9, and 12 were 227.3, 344.3, and 624.7 g, respectively, as listed in Table 3. In addition to 2 wk of pre-feeding, at least 5 d of force-feeding had been carried out for these samples which caused a sharp increase in liver weight along this period. This was sufficient to achieve steatosis with all hepatocytes filled with fat, and as observed in the histopathology analysis all samples showed steatosis grade 3. Ballooning might have been masked due to the presence of diffuse steatosis, and especially due to microsteatosis. Inflammation and fibrosis continued to increase with force-feeding and at day 12, all 3 samples had achieved inflammation grade 2 and fibrosis stage F1a. Variations in SWE properties between inflammation grade 1 (I1) and 2 (I2), as well as between fibrosis grade 0 (F0) and grade 1a (F1a), were compared in Figure 5. As can be seen, all properties (except SWS dispersion) more or less followed an increasing trend, that is, there was a slight increase in viscoelasticity of the tissue from I1 to I2, and from F0 to F1a. Properties like SWS, Young's modulus, viscosity, and shear modulus seemed to be more distinguishable at 75 Hz than at 202 Hz, the latter frequency revealing more variance. However, it should also be noted that the sample size was not large enough (I1: 4 samples, I2: 5 samples, F0: 3 samples, F1a: 6 samples) to confirm various statistical assumptions.

Histology images displayed changes in tissue structure along the force-feeding process. Force-feeding caused an increase in the fat fraction within the liver, which subsequently increased the hepatocyte size from day 5 to 12. Overall, the trends from in vivo measurements (Figures 2 and 3 along with Figure 4) revealed that the viscoelasticity of the liver tissue increased as the fat fraction increased.

Limitations

A few limitations can be pointed out. 1) This study was conducted on 9 mulard ducks, which is rather a small cohort for statistical interpretations. A larger cohort might be considered in a future study. Recently, Ormachea and Parker (2020) projected similar results with various SW elastography parameters in a study on the viscoelastic characterization of fatty tissues. 2) Another challenge of the current study was using an ultrasound scanner on alive ducks, and restricting their movements as they feared human touch. Two persons held the ducks on their back to control any animal movement, which would cause a poorer SNR on acquired data. The ducks were being raised for the commercial production of foie gras and the use of anesthesia was out of scope. 3) Computational challenges included accurate computations of SWS and attenuation, especially on the last 2 d of acquisitions as the ducks had developed macro-steatosis causing stronger attenuation of SW. The fattening of duck livers with such a forced feeding protocol was reported in Bonnefont et al. (2019), where the lipid content was shown to increase progressively from day 0 to 12. 4) Estimation of the fat fraction could not be performed in this study. Imbault et al. (2017) proposed utilizing the Green's function estimation-based approach for tissue fat fraction assessment. This could be a feature to consider in the future with duck fatty livers. We also intend to validate our work using QUS analysis to complement the SW elastography approach.

Clinical Translation of This Work

Ultrasound elastography studies have shown a steady increase in liver stiffness during fibrosis stages (Bavu et al., 2011; Palmeri et al., 2011). However, the effects of steatosis and inflammation on liver stiffness remain debatable. Yoneda et al. (2010) reported lower stiffness values in NAFLD patients with no fibrosis compared to healthy volunteers. Inflammation has been reported to slightly increase liver stiffness with inflammation grades in patients with mild fibrosis, but not in those with significant fibrosis (Zeng et al., 2015). On the other hand, Yoneda et al. (2010) and Palmeri et al. (2011) did not observe any correlation between liver stiffness and inflammation. Chen et al. (2011) reported that NAFLD patients with inflammation but no fibrosis had significantly higher liver stiffness compared to those with simple steatosis. Thus, it is expected that potential discrepancies in liver stiffness values may also arise due to the coexistence of steatosis, inflammation, and fibrosis in the NASH continuum. Most prior studies considered only stiffness as a biomarker while not exploiting the lossy nature of the liver. Thus, having more than 1 viscoelasticity biomarker could be useful to obtain more insight on liver parenchyma state. The animal model used in this study to investigate fatty liver stages in ducks with 6 viscoelasticity parameters may provide some insight on how to interpret future clinical studies on humans with NAFLD.

Potential Impact for Foie Gras Producers

Most farms rely on force-feeding of ducks and geese through a gavage mechanism for foie gras production.

During this process, the birds undergo liver swelling induced by hepatic steatosis. Several scientific boards have suggested that the practice of gavage is detrimental to animal welfare (European Commission, Scientific Committee on Animal Health and Animal Welfare, 1998). Recent practices allow the geese or ducks to naturally feed themselves as the birds start overeating to prepare for migration as a means to store energy in the form of liver fat.

However, farms producing naturally induced foie gras often observe that a significant number of birds do not develop enough fat in their liver with natural overfeeding. Since there is no available means to inspect the liver in vivo, often the sacrifice goes in vain, which has a commercial impact. Force-feeding is still used by several foie gras producers as it can provide high success for liver fat growth in birds. However, several legislations are in the process of banishing this form of production to promote alternative methods that do not include gavage (Council of Europe, Standing Committee of the European Convention for the Protection of Animals Kept for Farming Purposes, 1999). Therefore, an in vivo method for foie gras grading is of immense interest for producers. Our study aimed at providing such a means and we anticipate that it has the potential to provide technological solutions to promote naturally induced foie gras.

CONCLUSIONS

A multiparametric ultrasound SW elastography approach was proposed to monitor changes in the viscoelastic properties of liver tissues in ducks as they underwent 12 d of force-feeding. Nine mulard ducks were investigated in vivo at the farmhouse. Six viscoelastic parameters were computed to characterize liver steatosis and 4 of these parameters were reported for the first time. The livers became stiffer and more attenuating with fat growth. This animal study was intended to serve as a preclinical model for human studies. We foresee that this study may provide scientific tools to improve monitoring over time of livers in ducks and geese for the foie gras production industry.

ACKNOWLEDGMENTS

This work was supported by an Audace grant #2019-AUDC-263591 from the Fonds de Recherche du Québec. An Tang was supported by a research scholarship from the Fonds de Recherche du Québec en Santé and Fondation de l'Association des Radiologistes du Québec Junior 2 Salary Award (FRQS-ARQ #34939). We also thank Fernande Ouellet and Francis Laroche, the foie gras producers (farm "Rusé comme un canard," Granby, QC, Canada), Nathalie Vermette, the veterinarian who performed ultrasound examinations, and Boris Chayer and Marie-Hélène Roy-Cardinal for their technical support and advice.

DISCLOSURES

Authors have no conflict of interest to declare.

REFERENCES

Amador, C., M. W. Urban, S. Chen, and J. F. Greenleaf. 2012. Loss tangent and complex modulus estimated by acoustic radiation force creep and shear wave dispersion. Phys. Med. Biol. 57:1263.

Baeza, E., C. Marie-Etancelin, S. Davail, and C. Diot. 2013. La stéatose hépatique chez les palmipèdes. INRA Prod. Anim. 26:403–414.

Barry, C. T., Z. Hah, A. Partin, R. A. Mooney, K. H. Chuang, A. Augustine, A. Almudevar, W. Cao, D. J. Rubens, and K. J. Parker. 2014. Mouse liver dispersion for the diagnosis of early-stage fatty liver disease: a 70-sample study. Ultrasound Med. Biol. 40:704–713.

Barry, C. T., C. Hazard, Z. Hah, G. Cheng, A. Partin, R. A. Mooney, K. H. Chuang, W. Cao, D. J. Rubens, and K. J. Parker. 2015. Shear wave dispersion in lean versus steatotic rat livers. J. Ultrasound Med. 34:1123–1129.

Barry, C. T., B. Mills, Z. Hah, R. A. Mooney, C. K. Ryan, D. J. Rubens, and K. J. Parker. 2012. Shear wave dispersion measures liver steatosis. Ultrasound Med. Biol. 38:175–182.

Bavu, E., J. L. Gennisson, M. Couade, J. Bercoff, V. Mallet, M. Fink, A. Badel, A. Vallet-Pichard, B. Nalpas, M. Tanter, and S. Pol. 2011. Noninvasive in vivo liver fibrosis evaluation using supersonic shear imaging: a clinical study on 113 hepatitis C virus patients. Ultrasound Med. Biol. 37:1361–1373.

Bernard, S., S. Kazemirad, and G. Cloutier. 2016. A frequency-shift method to measure shear-wave attenuation in soft tissues. IEEE Trans. Ultrason. Ferroelectr. Freq. Control 64:514–524.

Bhatt, M., M. A. Moussu, B. Chayer, F. Destrempes, M. Gesnik, L. Allard, A. Tang, and G. Cloutier. 2019. Reconstruction of viscosity maps in ultrasound shear wave elastography. IEEE Trans. Ultrason. Ferroelectr. Freq. Control 66:1065–1078.

Bonekamp, S., A. Tang, A. Mashhood, T. Wolfson, C. Changchien, M. S. Middleton, L. Clark, A. Gamst, R. Loomba, and C. B. Sirlin. 2014. Spatial distribution of MRI-determined hepatic proton density fat fraction in adults with nonalcoholic fatty liver disease. J. Magn. Reson. Imaging 39:1525–1532.

Bonnefont, C. M., C. Molette, F. Lavigne, H. Manse, C. Bravo, B. Lo, H. Rémignon, J. Arroyo, and M. Bouillier-Oudot. 2019. Evolution of liver fattening and foie gras technological yield during the overfeeding period in mule duck. Poult. Sci. 98:5724–5733.

Bouchard, R. R., S. J. Hsu, P. D. Wolf, and G. E. Trahey. 2009. *In vivo* cardiac, acoustic-radiation-force-driven, shear wave velocimetry. Ultrason. Imaging 31:201–213.

Carrascal, C. A., S. Chen, A. Manduca, J. F. Greenleaf, and M. W. Urban. 2017. Improved shear wave group velocity estimation method based on spatiotemporal peak and thresholding motion search. IEEE Trans. Ultrason. Ferroelectr. Freq. Control 64:660–668.

Chen, S., W. Sanchez, M. R. Callstrom, B. Gorman, J. T. Lewis, S. O. Sanderson, J. F. Greenleaf, H. Xie, Y. Shi, M. Pashley, and V. Shamdasani. 2013. Assessment of liver viscoelasticity by using shear waves induced by ultrasound radiation force. Radiology 266:964–970.

Chen, J., J. A. Talwalkar, M. Yin, K. J. Glaser, S. O. Sanderson, and R. L. Ehman. 2011. Early detection of nonalcoholic steatohepatitis in patients with nonalcoholic fatty liver disease by using MR elastography. Radiology 259:749–756.

Cherry, E. 2016. Food, Chapter 5. Pages 58–74 in Culture and Activism: Animal Rights in France and the United States. Routledge, New York, NY.

Council of Europe, Standing committee of the European convention for the protection of animals kept for farming purposes (T-AP). 1999. Recommendation Concerning Muscovy Ducks (*cairina Moschata*) and Hybrids of Muscovyand Domestic Ducks (*anas Platyrhynchos*).

Deffieux, T., J. L. Gennisson, L. Bousquet, M. Corouge, S. Cosconea, D. Amroun, S. Tripon, B. Terris, V. Mallet, P. Sogni, and

M. Tanter. 2015. Investigating liver stiffness and viscosity for fibrosis, steatosis and activity staging using shear wave elastography. J. Hepatol. 62:317–324.
Deffieux, T., G. Montaldo, M. Tanter, and M. Fink. 2009. Shear wave spectroscopy for in vivo quantification of human soft tissues viscoelasticity. IEEE Trans. Med. Imag. 28:313–322.
Destrempes, F., and G. Cloutier. 2013. Review of envelope statistics models for quantitative ultrasound imaging and tissue characterization, Chapter 10. Pages 219–274 in Quantitative Ultrasound in Soft Tissues. J. Mammou and M. L. Oelze, eds. Springer, Dordrecht, The Netherlands.
Ferraioli, G., C. Tinelli, R. Lissandrin, M. Zicchetti, B. Dal Bello, G. Filice, and C. Filice. 2014. Point shear wave elastography method for assessing liver stiffness. World J. Gastroentero. 20:4787–4796.
European Commission, Scientific Committee on Animal Health and Animal Welfare (SCAHAW). 1998. Welfare aspects of the production of *foie gras* in ducks and geese. Accessed Feb. 2020. https://ec.europa.eu/food/sites/food/files/safety/docs/sci-com_scah_out17_en.pdf.
Franchi-Abella, S., L. Corno, E. Gonzales, G. Antoni, M. Fabre, B. Ducot, D. Pariente, J. L. Gennisson, M. Tanter, and J. M. Corréas. 2016. Feasibility and diagnostic accuracy of supersonic shear-wave elastography for the assessment of liver stiffness and liver fibrosis in children: a pilot study of 96 patients. Radiology 278:554–562.
Garcia, D., L. Le Tarnec, S. Muth, E. Montagnon, J. Porée, and G. Cloutier G. 2013. Stolt's f-k migration for plane wave ultrasound imaging. IEEE Trans. Ultrason. Ferroelectr. Freq. Control 60:1853–1867.
Gesnik, M., M. Bhatt, M. H. Roy-Cardinal, F. Destrempes, L. Allard, B. N. Nguyen, T. Alquier, J. F. Giroux, A. Tang, and G. Cloutier. 2020. *In vivo* ultrafast quantitative ultrasound and shear wave elastography imaging on farm-raised duck livers during force feeding. Ultrasound Med. Biol. 7:1715–1726.
Gharib, A. M., M. A. Han, E. G. Meissner, D. E. Kleiner, X. Zhao, M. McLaughlin, L. Matthews, B. Rizvi, K. Z. Abd-Elmoniem, R. Sinkus, and E. Levy. 2017. Magnetic resonance elastography shear wave velocity correlates with liver fibrosis and hepatic venous pressure gradient in adults with advanced liver disease. Biomed. Res. Int. 2017:1–8.
Han, A., A. S. Boehringer, Y. N. Zhang, V. Montes, M. P. Andre, J. W. Erdman, R. Loomba, C. B. Sirlin, and D. W. O'Brien. 2019. Improved assessment of hepatic steatosis in humans using multiparametric quantitative ultrasound. IEEE Int. Ultrason. Symp. 1819–1822.
Imbault, M., A. Faccinetto, B. F. Osmanski, A. Tissier, T. Deffieux, J. L. Gennisson, V. Vilgrain, and M. Tanter. 2017. Robust sound speed estimation for ultrasound-based hepatic steatosis assessment. Phys. Med. Biol. 62:3582–3598.
Kazemirad, S., S. Bernard, S. Hybois, A. Tang, and G. Cloutier. 2016. Ultrasound shear wave viscoelastography: model-independent quantification of the complex shear modulus. IEEE Trans. Ultrason. Ferroelectr. Freq. Control 63:1399–1408.
Kleiner, D. E., E. M. Brunt, M. Van-Natta, C. Behling, M. J. Contos, O. W. Cummings, L. D. Ferrell, Y. C. Liu, M. S. Torbenson, A. Unalp-Arida, and M. Yeh. 2005. Design and validation of a histological scoring system for nonalcoholic fatty liver disease. Hepatology 41:1313–1321.
Litt, J., C. Leterrier, D. Savietto, and L. Fortun-Lamothe. 2020. Influence of dietary strategy on progression of health and behaviour in mule ducks reared for fatty liver production. Animal 14:1258–1269.
Loupas, T., J. T. Powers, and R. W. Gill. 1995. An axial velocity estimator for ultrasound blood flow imaging, based on a full evaluation of the Doppler equation by means of a two-dimensional autocorrelation approach. IEEE Trans. Ultrason. Ferroelectr. Freq. Control 42:672–688.
Loomba, R. 2018. Role of imaging-based biomarkers in NAFLD: recent advances in clinical application and future research directions. J. Hepatol. 68:296–304.
Nenadic, I. Z., B. Qiang, M. W. Urban, H. Zhao, W. Sanchez, J. F. Greenleaf, and S. Chen. 2017. Attenuation measuring ultrasound shear wave elastography and in vivo application in post-transplant liver patients. Phys. Med. Biol. 62:484–500.
Nightingale, K. R., N. C. Rouze, S. J. Rosenzweig, M. H. Wang, M. F. Abdelmalek, C. D. Guy, and M. L. Palmeri. 2015. Derivation and analysis of viscoelastic properties in human liver: impact of frequency on fibrosis and steatosis staging. IEEE Trans. Ultrason. Ferroelectr. Freq. Control 62:165–175.
Ormachea, J., and K. J. Parker. 2020. Comprehensive viscoelastic characterization of tissues and the inter-relationship of shear wave (group and phase) velocity, attenuation and dispersion. Ultrasound Med. Biol. 46:3448–3459.
Osaki, A., T. Kubota, T. Suda, M. Igarashi, K. Nagasaki, A. Tsuchiya, M. Yano, Y. Tamura, M. Takamura, H. Kawai, and S. Yamagiwa. 2010. Shear wave velocity is a useful marker for managing nonalcoholic steatohepatitis. World J. Gastroentero. 16:2918–2925.
Palmeri, M. L., M. H. Wang, N. C. Rouze, M. F. Abdelmalek, C. D. Guy, B. Moser, A. M. Diehl, and K. R. Nightingale. 2011. Non-invasive evaluation of hepatic fibrosis using acoustic radiation force-based shear stiffness in patients with nonalcoholic fatty liver disease. J. Hepatol. 55:666–672.
Palmeri, M. 2019. RSNA/QIBA efforts to standardize shear wave speed as a biomarker for liver fibrosis staging. Ultrasound Med. Biol. 45:S24.
Park, C. C., P. Nguyen, C. Hernandez, R. Bettencourt, K. Ramirez, L. Fortney, J. Hooker, E. Sy, M. T. Savides, M. H. Alquiraish, and M. A. Valasek. 2017. Magnetic resonance elastography vs transient elastography in detection of fibrosis and noninvasive measurement of steatosis in patients with biopsy-proven nonalcoholic fatty liver disease. Gastroenterology 152:598–607.
Parker, K. J., A. Partin, and D. J. Rubens. 2015. What do we know about shear wave dispersion in normal and steatotic livers? Ultrasound Med. Biol. 41:1481–1487.
Parker, K. J., J. Ormachea, S. Will, and Z. Hah. 2018. Analysis of transient shear wave in lossy media. Ultrasound Med. Biol. 44:1504–1515.
Qu, Y., M. Li, G. Hamilton, Y. N. Zhang, and B. Song. 2019. Diagnostic accuracy of hepatic proton density fat fraction measured by magnetic resonance imaging for the evaluation of liver steatosis with histology as reference standard: a meta-analysis. Europ. Radiol. 29:5180–5189.
Ricci, C., R. Longo, E. Gioulis, M. Bosco, P. Pollesello, F. Masutti, L. S. Crocè, S. Paoletti, B. de Bernard, C. Tiribelli, and L. Dalla Palma. 1997. Noninvasive in vivo quantitative assessment of fat content in human liver. J. Hepatol. 27:108–113.
Rouze, N. C., M. L. Palmeri, and K. R. Nightingale. 2015. An analytic, Fourier domain description of shear wave propagation in a viscoelastic medium using asymmetric Gaussian sources. J. Acoust. Soc. Am. 138:1012–1022.
Sandrin, L., B. Fourquet, J. M. Hasquenoph, S. Yon, C. Fournier, F. Mal, C. Christidis, M. Ziol, B. Poulet, F. Kazemi, and M. Beaugrand. 2003. Transient elastography: a new noninvasive method for assessment of hepatic fibrosis. Ultrasound Med. Biol. 29:1705–1713.
Sanyal, A. J., E. M. Brunt EM, D. E. Kleiner, K. V. Kowdley, N. Chalasani, J. Lavine, V. Ratziu, and A. McCullough. 2011. Endpoints and clinical trial design for nonalcoholic steatohepatitis. Hepatology 54:344–353.
Sharma, A. K., J. Reis, D. C. Oenheimer, D. J. Rubens, J. Ormachea, Z. Hah, and K. J. Parker. 2019. Attenuation of shear waves in normal and steatotic livers. Ultrasound Med. Biol. 45:895–901.
Song, P., D. C. Mellema, S. P. Sheedy, D. D. Meixner, R. M. Karshen, M. W. Urban, A. Manduca, W. Sanchez, M. R. Callstrom, J. F. Greenleaf, and S. Chen. 2016. Performance of 2-dimensional ultrasound shear wave elastography in liver fibrosis detection using magnetic resonance elastography as the reference standard: a pilot study. J. Ultrasound Med. 35:401–412.
Yoneda, M., K. Suzuki, S. Kato, K. Fujita, Y. Nozaki, K. Hosono, S. Saito, and A. Nakajima. 2010. Nonalcoholic fatty liver disease: US-based acoustic radiation force impulse elastography. Radiology 256:640–647.
Yoon, J. H., J. M. Lee, J. K. Han, and B. I. Cho. 2014. Shear wave elastography for liver stiffness measurement in clinical sonographic examinations: evaluation of intraobserver reproducibility, technical failure, and unreliable stiffness measurements. J. Ultrasound Med. 33:437–447.

Zeng, X., C. Xu, D. He, H. Zhang, J. Xia, D. Shi, L. Kong, X. He, and Y. Wang. 2015. Influence of hepatic inflammation on FibroScan findings in diagnosing fibrosis in patients with chronic hepatitis B. Ultrasound Med. Biol. 41:1538–1544.

Zeldovich, L. 2019. Farmers and chefs think there may be an ethical future for foie gras. Quartz. Accessed Feb. 2020. https://qz.com/1750093/farmers-and-chefs-think-there-may-be-an-ethical-future-for-foie-gras/.